

# Optofluidic control of the dispersion of nanoscale dumbbells

M. Meléndez,<sup>1,\*</sup> N. Alcázar Cano,<sup>1</sup> R. P. Peláez,<sup>1</sup> J. J. Sáenz,<sup>2,3</sup> and R. Delgado-Buscalioni<sup>1,4</sup>

<sup>1</sup>Universidad Autónoma de Madrid, 28049, Madrid, Spain.

<sup>2</sup>Donostia International Physics Center (DIPC),

Paseo Manuel Lardizabal 4, 20018, Donostia-San Sebastian, Spain.

<sup>3</sup>IKERBASQUE, Basque Foundation for Science, 48013 Bilbao, Spain.

<sup>4</sup>Condensed Matter Physics Center (IFIMAC), Universidad Autónoma de Madrid, 28049 Madrid, Spain.

(Dated: today)

Previous research has shown that gold nanoparticles immersed in water in an optical vortex lattice formed by the perpendicular intersection of two standing light waves with a  $\pi/2$  rad phase difference will experience enhanced dispersion that scales with the intensity of the incident laser. We show that flexible nanoscale dumbbells (created by attaching two such gold particles by means of a polymer chain) in the same field display different types of motion depending on the chain length and field intensity. We have not disregarded the secondary optical forces due to light scattering. The dumbbells may disperse, rotate or remain trapped. For some values of the parameters, the (enhanced) dispersion possesses a displacement distribution with exponential tails, making the motion anomalous, though Brownian.

Optofluidics faces the challenging problem of understanding the interactions of light waves, electrons, and fluid and solid matter at the micro- and nanoscale. Previous work has shown that it can provide a way to control the transport properties of nanoscale objects, and it has already been applied to the guiding and sorting of particles in microfluidic flows [1, 2].

Numerical experiments have shown how to control the magnitude of the mean square displacement in a dilute suspension of gold nanoparticles in water by creating a stationary optical field at the intersection of two coherent laser beams with wavelengths close to the plasmon resonance ( $\lambda \approx 395$  nm) [3, 5]. In particular, Albaladejo *et al.* demonstrated that perpendicular beams with a phase lag of  $\pi/2$  rad enhance the dispersion of nanoparticles by a factor proportional to the power density of the laser [3].

We aim here to provide a method for tuning the dispersion properties of nanoscale dumbbells created by attaching two identical 50 nm-radius gold spheres by means of a polymer strand [4]. Even though the setup in [3] enhances the dispersion for gold nanoparticles, the mean square displacement for dumbbells depends critically on the field intensity and the length of the connecting strand compared to the wavelength, as we shall show below. We will use the term diffusion to refer to *thermal* diffusion caused by random molecular collisions, and dispersion to refer to the combined effect of thermal fluctuations, optical forces and hydrodynamic coupling.

## SIMULATION SETUP

Following Ref. [3], we began with a nonconservative optical field generated in water by the intersection of two perpendicular coherent laser beams with a  $\pi/2$  rad phase difference polarised along the  $z$  axis. The resulting force field acting on gold nanoparticles along the  $xy$

plane,  $\mathbf{F}_{opt}(x, y)$ , an optical vortex lattice (Fig. 1), corresponded to the equation below,

$$\mathbf{F}_{opt} = 2\alpha' \frac{n}{c} I \nabla (\sin(kx) + \sin(ky))^2 + 2\alpha'' \frac{n}{c} I \nabla \times (2 \cos(kx) \cos(ky) \mathbf{e}_z). \quad (1)$$

The refractive index was set to  $n = \sqrt{1.8}$ . We assumed that the particle radii are small enough compared to the incident wavelength to treat the particles as electric dipoles with a moment given by  $\mathbf{p} = \epsilon \epsilon_0 \alpha \mathbf{E}$ , with complex electric polarisability  $\alpha = \alpha' + i\alpha''$  and total field  $\mathbf{E}$ . We used  $k = nk_0 = n2\pi/\lambda$  for the wave-number of the incident laser light, close to the gold plasmon resonance in water, which gives a wavelength of  $\lambda \approx 395$  nm. For these values  $\alpha' \approx 1 \times 10^{-21} \text{ m}^3$  and  $\alpha'' \approx 2\alpha'$ . For an incident electric field  $\mathbf{E}_0$ , the field intensity considered here,  $(1/2)\epsilon_0 c n |\mathbf{E}_0|^2 \sim 10^9 \text{ W/m}^2$ , could be achieved by focusing a 0.1 W laser onto a  $(10 \mu\text{m})^2$  region. We have used  $c$  to represent the speed of light and  $\mathbf{u}_z$  for the unit vector in the direction perpendicular to the  $xy$  plane. According to Eq. (1), the energy from the light shone on a gold nanoparticle is typically  $U \equiv 2I \frac{n}{c} \alpha'$ . For the 50 nm-radius gold particles, experimentally feasible laser intensities lie in the  $U \in [0 - 10^2] k_B T$  range at  $T = 300$  K, with  $U \simeq 1.7 k_B T$  for the aforementioned 0.1 W laser.

Our flexible dumbbells consist of a chain of  $N$  spheres connected with standard finitely extensible nonlinear elastic (FENE) bonds [6]. In addition, we have included semiflexible potentials to simulate the rigidity of the polymer [7] and Weeks-Chandler-Andersen (WCA) interactions among the beads to account for excluded volume effects [8]. We chose a persistence length of  $l_p = 50$  nm, typical of double-stranded DNA, though changes in the range of 50–5000 nm did not significantly alter the dispersion of the 100–1000 nm-length chains of interest to this study (mean square displacements changed by less than a factor of two). The beads at the two ends of the

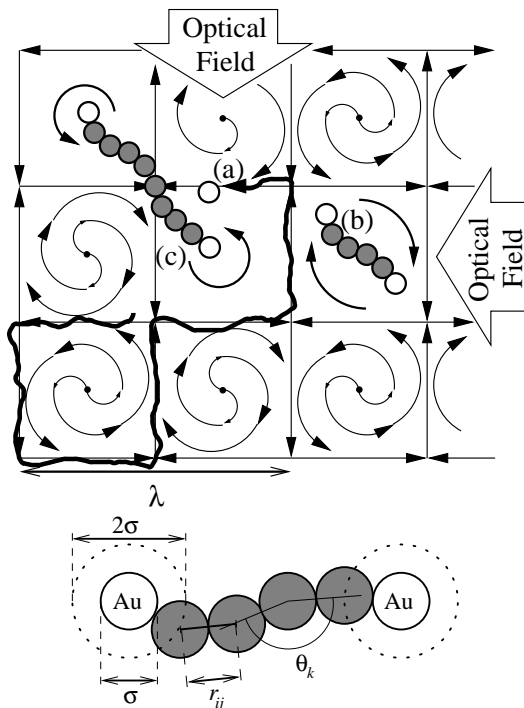


FIG. 1. Simplified representation of the forces in the optical vortex lattice in Eq. (1). A single gold particle (a) experiences enhanced dispersion. Short dumbbells follow similar trajectories. We can easily trap the dumbbells (b) and (c) using one or two vortices if we neglect hydrodynamic interactions. *Below*: Schematic drawing of a flexible dumbbell. Two gold particles attached by means of a FENE bead-spring chain (which limits the interparticle separation  $r_{ij} < 3r$ , where  $r$  is the radius of a bead) interact with an optical force field. WCA interactions with diameter  $\sigma$  model excluded volume effects. An extra coat of transparent material (dotted lines) was included in some of the simulations. Angular springs between consecutive links oppose bending and tend to restore the angles to  $\theta_k = \pi$  rad.

chain represent gold nanoparticles subject to the optical forces in Eq. (1) (see Fig. 1). Most of the simulations added the effect of light scattering off the end particles [17]. In these cases we included an extra coat of transparent material (represented with dotted lines in the figure) mimicking the experiments in Ref. [9], which prevented the gold spheres from coming too close to each other as that would make the approximations involved in the calculation of the scattering unsound. If the coat were removed, the equations of both the forces and the optical scattering would have to be modified for small separations, and the possibility of particle merging would have to be taken into account.

For the time scales of interest here, Brownian dynamics (overdamped Langevin equations of motion) accurately describe the fluctuating motion of our nanoscale dumbbells [10]. Using  $\mathbf{R}$  to represent a vector of all the coordinates, a realisation of the particle trajectories cor-

responds to the solution of the following stochastic differential equation [11], which we integrated numerically with an Euler-Maruyama scheme.

$$d\mathbf{R} = \mathbf{M}\mathbf{F} dt + \sqrt{2k_B T}\mathbf{B} d\mathbf{W}. \quad (2)$$

The first term on the right stands for the deterministic flow, with the mobility tensor  $\mathbf{M}$  multiplying the net force  $\mathbf{F}$ , which includes the optical forces in Eq. (1), the WCA interaction among beads, the FENE bonds and the semiflexible potential. The last term incorporates the effect of thermal fluctuations through a random force.  $\mathbf{B}$  satisfies the relation  $\mathbf{B}\mathbf{B}^T = \mathbf{M}$ ,  $d\mathbf{W}$  is the Wiener process, and  $k_B T$  is Boltzmann's constant multiplied by the temperature.

By using the Rotne-Prager-Yamakawa tensor [13, 14] as a mobility matrix, you can model hydrodynamic interaction among the particles. The  $\mathbf{B}$  matrix was calculated with the usual algorithm for Cholesky decomposition [15]. In some of our simulations, though, we disregarded hydrodynamic interactions altogether. In that case,  $\mathbf{M}$  equals the identity matrix multiplied by  $\gamma^{-1}$ , the inverse of the friction coefficient, and the calculation of  $\mathbf{B}$  becomes trivial. Comparing the latter purely Brownian simulations to the other results allowed us to isolate the effects due to hydrodynamics.

In addition to hydrodynamic interactions, a realistic simulation of the moving dumbbells must include the secondary forces arising from the light scattered by the gold particles. Besides the incident field  $\mathbf{E}_0$ , the total electric field  $\mathbf{E}$  at the position of particle  $i$ ,  $\mathbf{r}_i$  must then include a contribution from scattering proportional to the Green's function propagator  $\mathbf{G}(r_i, r_j)$  at the position of other particles [16] multiplied by the total field at those locations  $r_j$ , that is to say,

$$\mathbf{E}(\mathbf{r}_i) = \mathbf{E}_0(\mathbf{r}_i) + k^2 \sum_{j \neq i} \mathbf{G}(\mathbf{r}_i, \mathbf{r}_j) \alpha \mathbf{E}(\mathbf{r}_j). \quad (3)$$

By solving the equation above numerically for  $\mathbf{E}(\mathbf{r}_i)$  [17] and inserting the result into the expression for the force, we obtain the force on particle  $i$  [18].

$$\mathbf{F}_{opt}(\mathbf{r}_i) = \frac{\epsilon\epsilon_0}{2} \text{Re}(\alpha \mathbf{E}(\mathbf{r}_i) \cdot \nabla \mathbf{E}^*(\mathbf{r}_i)). \quad (4)$$

This means that component  $\mu$  of the average force on particle  $i$  equals

$$(F_{opt}(\mathbf{r}_i))_\mu = \frac{\epsilon\epsilon_0}{2} \text{Re} \left( \alpha \sum_\nu E_\nu(\mathbf{r}_i) \frac{\partial}{\partial x_\mu} E_\nu^*(\mathbf{r}_i) \right). \quad (5)$$

Therefore, Eq. (4) replaces Eq. (1) when the simulations take light scattering into account. As we will show below, scattering alters the motion of the dumbbells qualitatively.

## RESULTS

The schematic representation of the optical field (1) shown in Fig. 1 indicates the direction of the forces acting on a single nanoparticle due to the incident laser beams. The particles (and, one might expect, chains much shorter than the wavelength) follow the lines of force and experience enhanced dispersion [3] moving from one unstable node to another. Attaching two gold spheres alters the picture, because they may become entrapped by vortices for certain values of the parameters, as illustrated in Fig. 1. For example, *when we neglect hydrodynamic interactions*, relatively rigid 10-bead chains display enhanced dispersion when the laser wavelength equals 100 times the radius of the gold particles, but remain trapped, rotating in a vortex, when the wavelength approximately doubles the length of the dumbbell (as in Fig. 1b), even when the program includes the effects of light scattering ( $r = 50$  nm,  $U = 10 k_B T$  and persistence length  $l_p = 1000 r$ ). Similarly, dispersion plummets when the wavelength approaches the length of the chain, which remains stuck between two vortices, with both ends rotating in the same direction (Fig. 1c). Not much changes when we reduce the persistence length to that of dsDNA, except that at the larger values of the wavelength ( $\lambda = 50\text{--}100$ ) the chains show a greater tendency to fold in half and remain circling a vortex, but the secondary scattering eliminates this effect.

Notwithstanding the interest of this dynamical behaviour, here we have chosen to concentrate on realistic values of the parameters, considering current experimental technology. As mentioned above, the optical field for  $r = 50$  nm gold particles has a wavelength  $\lambda \approx 4r$ . This implies that dumbbells short enough to lie in a vortex feel strong forces due to light scattering off the ends, which significantly modify the force landscape. For instance, 4-bead dumbbells tend to move to a nearby saddle point and sit there (Fig. 2). We observed the same behaviour when the intermediate FENE chain was approximated by means of a single harmonic bond.

*Adding hydrodynamics* into the mix induces coupling among the bead displacements, and this has a significant effect on the dynamics, as the mutual drag pulls the dumbbells out of the vortices. The hydrodynamic interaction between two nearby nanoparticles in a vortex lattice has been analysed in Ref. [17]. Fig. 3 charts the scaled dispersion coefficient  $D$  of a dumbbell as a function of two parameters: the laser intensity and the chain length, with  $D = \langle \Delta x^2 + \Delta y^2 \rangle / (4\Delta t)$ , and  $\Delta x = x(t + \Delta t) - x(t)$  and  $\Delta y = y(t + \Delta t) - y(t)$ , and  $D_{th}$  representing the thermal diffusion coefficient with the optical fields switched off. The colour scale values shown in Fig. 3 were calculated by interpolation. We can still find a region, indicated by the blue area in Fig. 3, in which the dumbbells remain trapped on saddle points according to

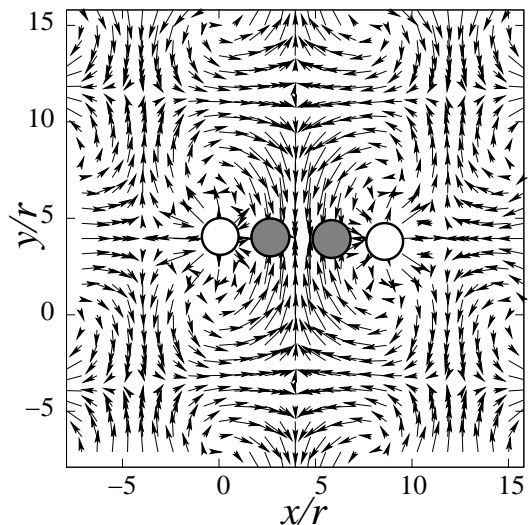


FIG. 2. Dumbbell sitting in a saddle due to the combined effect of the incident laser field and light scattering off the gold particles at the ends ( $\lambda = 7.9 r$ ,  $U = 10 k_B T$ ). Note that the optical forces stretch the chain.

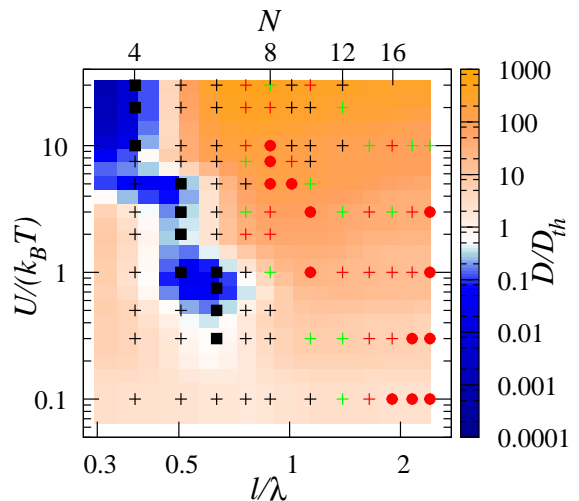


FIG. 3. Dispersion coefficient  $D$  divided by thermal diffusion  $D_{th}$  for different values of the laser intensity and dumbbell length. The colour scale values were obtained by interpolation. Points mark the values of the parameters for which simulations were performed. See Fig. 4) for an explanation of the meaning of the differences among points.  $D_{th}$  was calculated numerically for each length by switching off the laser forces.

the mechanism shown in Fig. 2. Close to this region, approximately for  $\lambda \approx l$ , we observe a strong enhancement of dispersion (marked with red circles in Fig. 3) as also evidenced in Fig. 4. For  $\lambda > l$ ,  $D$  scales very roughly as  $D/D_{th} \propto U^{0.84}/l$  (corresponding to points marked with crosses, see also Fig. 4).

Fig. 5 displays the mean square displacement of a moving dumbbell on the  $xy$  plane for different time scales.

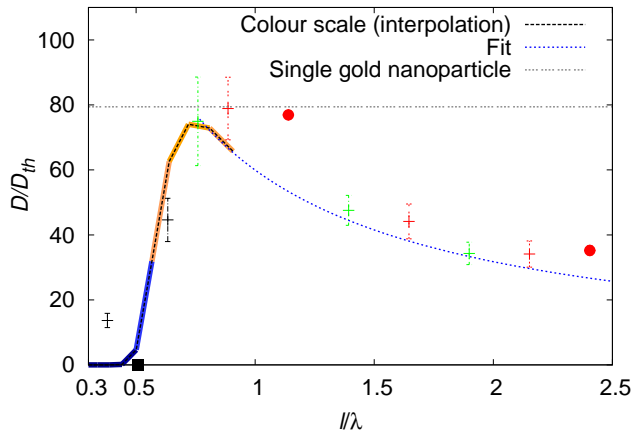


FIG. 4. Dispersion coefficient  $D$  divided by thermal diffusion  $D_{th}$  for different dumbbell lengths. This figure presents a horizontal section of Fig. 3 for  $U = 3 k_B T$ . Red points lie above a fitted function  $D_{fit} \propto U^{0.84}/l$  and black values below. Green points coincide with the fit within their margin of error. Squares correspond to trapped dumbbells ( $D/D_{th} < 0.1$ ) and circles to dumbbells with dispersion coefficients greater than  $D_{fit}$  by at least 20%. We also show the value of  $D/D_{th}$  for a single gold nanoparticle in the same optical force field. The fit resulted from approximating all the simulations shown in Fig. 3, not just the ones shown here.

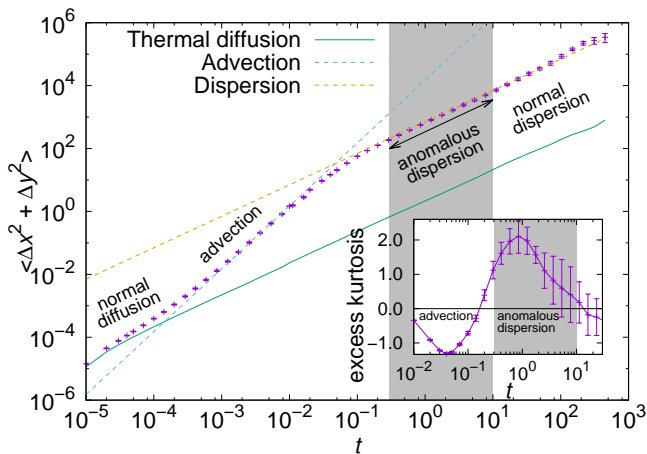


FIG. 5. Mean square displacement in units of  $\sigma^2$  for an  $N = 8$  dumbbell at  $U = 7.5 k_B T$  (points) showing the transition from thermal diffusion at short times to enhanced dispersion at long times (measured in Brownian time units  $\sigma^2/D_{th}$ ). Anomalous Brownian motion was observed for times in the range 0.3–10 (shaded area). The inset shows that the excess kurtosis for the displacement distribution becomes positive in the same range.

The general shape of the curve coincides with that of a single gold particle, with Brownian motion at short and long time intervals connected by means of an advective regime at intermediate time scales. Below the mean free time of molecular collisions (not shown in the figure) the

physical system would move in a ballistic regime, with the mean square displacement proportional to the time squared. At larger time scales, we find thermal diffusion. Because the optical forces push the gold nanoparticles from one saddle node to the next, the dumbbell then encounters an advective regime, where the mean square displacement scales once again with  $t^2$ . Finally, at long times the motion of the dumbbell behaves like diffusion, but with a larger diffusion coefficient. In some cases, including that of Fig. 5 ( $N = 8$ ,  $U = 7.5 k_B T$ ), we found anomalous Brownian motion for a range of times, in contrast to the case of single nanoparticles. This non-Gaussian character of the displacements cannot be seen in the graph of the mean square displacement, but is confirmed by the inset in Fig. 5, which plots the excess kurtosis for the displacement distribution and reveals that it becomes positive in the range of anomalous Brownian motion. If we disregard hydrodynamic interactions, the anomalous character of the motion disappears.

For strict thermal diffusion, the dumbbell  $D_{th}$  decreases with the length of the chain, but for the phenomenon studied here, the dispersion in some cases approached that of single nanoparticles (Fig. 4).

The probability distribution function for the size of a step in a two-dimensional random walk follows a Maxwell-Boltzmann curve

$$P(r_{\Delta t}) = \frac{r_{\Delta t}}{\sigma^2} e^{-r_{\Delta t}^2/(2\sigma^2)}, \quad (6)$$

with  $r_{\Delta t}$  a shorthand for  $\|\mathbf{r}(t + \Delta t) - \mathbf{r}(t)\|$ . This function may be viewed as the self contribution to the radial van Hove function for a time delay equal to  $\Delta t$ . Single nanoparticles on the vortex lattice follow a jagged version of this distribution and some values of the parameters for dumbbells produce similar distributions ( $N = 12, 16$ ,  $U^* = 3$  in Fig. 6). Contrast the trend along the tail of the distributions to the behaviour near regions marked with red dots in Fig. 3 ( $N = 8$ ,  $U^* = 3, 5$ ), which fall off exponentially, indicating the anomalous (though still Brownian) nature of the diffusive motion in these cases [19]. The data in Fig. 6 were all obtained from time lags  $\Delta t$  for which the in-plane dispersion coefficient  $D_{th}$  had reached a plateau. For larger values of the time lag, the distribution reverted to the standard Gaussian Maxwell-Boltzmann statistics [20, 21]. Accordingly, despite the superficial resemblance to Lévy walks [22], the long-time dynamics follow normal random walk statistics. A comparison with simulations without scattering revealed that scattering, in fact, postpones the arrival of Gaussian distributions.

The higher-than-normal probability of a large displacement, compared to Gaussian statistics, emerges from a tendency to move along the  $x = \pm y$  diagonal directions in the lattice due to hydrodynamic interactions [17] and can be spotted easily by comparing the trajectory of the Gaussian displacements on the left of Fig. 7 to that of

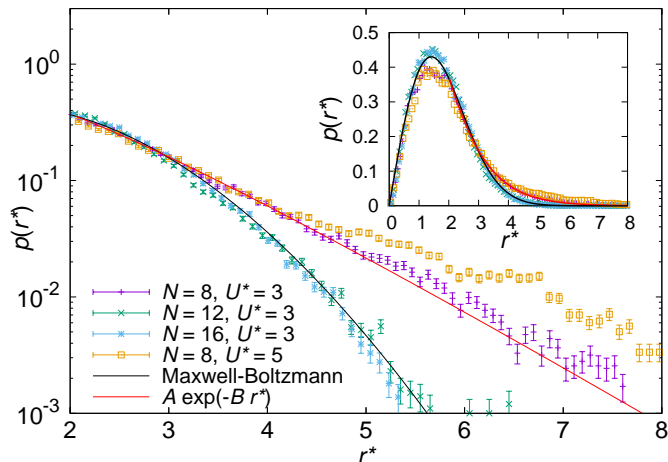


FIG. 6. Probability density function tails for the displacement of diffusing dumbbells on a semi-logarithmic scale. The horizontal axis represents a scaled step  $r^* = r_{\Delta t} / \sqrt{(U^*/n)\Delta t}$ , with  $\Delta t = 100 \sigma^2 / D_{th}$ . The inset shows the distributions on a linear scale. The number of beads  $N$  includes the gold nanoparticles.  $U^*$  means  $U/(k_B T)$ . This function represents the dumbbell contribution to the radial van Hove function for a fixed time delay  $\Delta t$ .

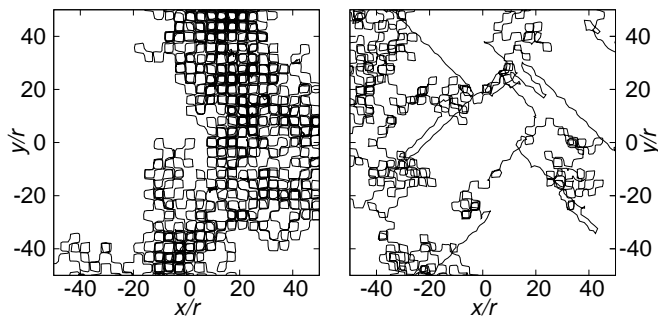


FIG. 7. Centre of mass trajectories of a dumbbell in an optical vortex lattice ( $U = 7.5 k_B T$ ). The  $N = 5$  dumbbell on the left displays normal (Gaussian) enhanced Brownian displacements at long times, while the  $N = 8$  dumbbell on the right has a non-Gaussian displacement distribution function due to the higher probability of a long displacement along one of the  $x = \pm y$  diagonals caused by hydrodynamic drag.

an anomalous Brownian process (Fig. 7, right). In contrast, single nanoparticles do not prefer to move along diagonals. They simply move to the next saddle node and randomly choose one of two opposite directions, alternating up/down with left/right.

#### LIMITATIONS OF THE PRESENT APPROACH

The fact that optical absorption induces heating in the gold nanoparticles [23] places an upper bound on the intensity of the laser source. The phenomena de-

scribed in our paper would obviously change dramatically if the heating caused the water to boil around the particles. Previous research has reported such a formation of vapour bubbles [24, 25]. The water in contact with the metal sphere would increase its temperature by an amount proportional to the square of the sphere radius  $r$  and the laser intensity  $I$  [24],

$$\Delta T_{max} \propto r^2 I. \quad (7)$$

The data provided in [24] allow us to estimate a temperature increase  $\Delta T \approx 120$  K for our  $10^9$  W/m<sup>2</sup> laser and 50 nm-radius sphere. However, this analytical solution neglects several effects due to the temperature dependence of optical and thermal properties of the gold particles, which all lead to an overestimation of  $\Delta T$  in the case of gold nanoparticles in water [26]. However, the combined heating effect of several particles would indeed lead to much higher temperatures [24, 25], and this sets a limit on the maximum volume fraction for which the present analysis holds. Nevertheless, temperature gradients around the nanoparticles might still have an effect on their motion due to thermophoresis [27], even below the boiling temperature.

Lastly, we would like to emphasise that we have focussed on the dynamics of a single dumbbell. At high enough concentrations of suspended dumbbells, hydrodynamic interactions would distort their motion, and the flows created by a moving dumbbell would affect the others, giving rise to collective dynamics, as proven in a previous work [17].

#### CONCLUSIONS

Nanoscale dumbbells, created by attaching two 50-nm-radius gold spheres by means of a polymer chain, enrich the dynamics predicted by Albadalejo *et al.* for nanoparticles in an optical vortex lattice [3]. Not only might they experience enhanced dispersion for large values of the laser intensity, but they can be trapped in a fixed position or be made to rotate (when  $l/\lambda \approx 0.5$ ). The different behaviours depend on the ratio of the chain length to the wavelength  $l/\lambda$  and the intensity of the incident lasers creating the vortex field.

As displayed in Fig. 3, relatively modest changes in the size of the chains or the laser intensity may lead to huge variations of the dispersion of dumbbells along the plane spanned by the direction of the lasers, and this provides a way to guide, filter or trap the dumbbells by tuning the intensity of the lasers.

#### ACKNOWLEDGEMENTS

We would like to thank J. Luis-Hita for his code to calculate the optical forces. This research was funded

by the Spanish MINECO project FIS2017-86007-C3-1-p, the MINECO and European Regional Development Fund project FIS2015-69295-C3-3-P, Explora Ciencia FIS2013-50510-EXP, and the Basque Department of Education project PI-2016-1-0041.

---

\* marc.melendez@uam.es

- [1] M. P. MACDONALD, G. C. SPALDING, and K. Dholakia, *Nature*, **426**, 421–424 (2003).
- [2] K. XIAO, D. G. GRIER, *Physical Review E* **82**, 051407 (2010).
- [3] S. ALBALADEJO, M. I. MARQUÉS, F. SCHEFFOLD, and J. J. SÁENZ, *Nano Letters*, **9(10)**, 3527–3531 (2009).
- [4] M. P. BUSSON, B. ROLLY, B. STOUT, E. LARQUET, A. POLMAN, and S. BIDAULT, *Nano Letters* **11**, 11, 5060–5065.
- [5] I. ZAPATA, R. DELGADO-BUSCALIONI, and J. J. SÁENZ, *Physical Review E*, **93(6)**, 062130 (2016).
- [6] H. R. WARNER JR, *Industrial & Engineering Chemistry Fundamentals*, **11(3)**, 379–387 (1972).
- [7] J. KIERFELD, O. NIAMPLOY, V. SA-YAKANIT, and R. LIPOWSKY, *The European Physical Journal E: Soft Matter and Biological Physics*, **14(1)**, 17–34 (2004).
- [8] H. C. ANDERSEN, J. D. WEEKS, and D. CHANDLER, *Physical Review A*, **4(4)**, 1597 (1971).
- [9] M. HONDA, Y. SAITO, N. I. SMITH, K. FUJITA, and S. KAWATA, *Optics Express* **19(13)**, 12375 (2011).
- [10] M. FIXMAN, *The Journal of Chemical Physics* **69.4**, 1527–1537 (1978).
- [11] P. S. DOYLE, and P. T. UNDERHILL, in *Handbook of Materials Modeling*, edited by S. YIP (Springer, 2005), p. 2619–2630.
- [12] P. E. KLOEDEN, and E. PLATEN, *Numerical Solution of Stochastic Differential Equations* (Springer, 2013) p. 305ff.
- [13] J. ROTNE, and S. PRAGER, *The Journal of Chemical Physics* **50.11** 4831–4837 (1969).
- [14] H. YAMAKAWA, *The Journal of Chemical Physics* **53.1** 436-443 (1970).
- [15] G. HÄMMERLIN, and K. H. HOFFMANN, *Numerical Mathematics*, Springer, p. 62 (2012).
- [16] L. NOVOTNY, and B. HECHT, *Principles of Nano-Optics*, Cambridge University Press (2006).
- [17] R. DELGADO-BUSCALIONI, M. MELÉNDEZ, J. LUIS-HITA, M. I. MARQUÉS and J. J. SÁENZ, *Physical Review E* **98**, 062614 (2018).
- [18] J. LUIS-HITA, J. J. SÁENZ, and M. I. MARQUÉS, *ACS Photonics* **3**, 7, 1286–1293 (2016).
- [19] B. WANG, M. ANTHONY, S. C. BAE, and S. GRANICK, *PNAS* **106** (36) 15160–15164 (2009).
- [20] B. WANG, J. KUO, S. C. BAE, and S. GRANICK, *Nature Materials* **11.6**, 481 (2012).
- [21] M. V. CHUBYSKY, and G. W. SLATER, *Physical Review Letters* **113**, 098302 (2014).
- [22] V. ZABURDAEV, S. DENISOV, and J. KLAFTER *Reviews of Modern Physics* **87**, 473 (2015).
- [23] Y. SEOL, A. E. CARPENTER, T. T. PERKINS, *Optics Letters* **31**, 16 2429–2431 (2006).
- [24] A. O. GOVOROV, H. H. RICHARDSON, *Nano Today* **2**, 30–38 (2007).
- [25] O. A. YESCHENKO, N. V. KUTSEVOL, A. P. NAUMENKO *Plasmonics* **11**, 345–350 (2016).
- [26] Y. SIVAN, S. CHU, *Nanophotonics* **6**: 317–328 (2017).
- [27] R. PIAZZA, *Journal of Physics: Condensed Matter* **16**, S4195 (2004).